Journal of Materials Chemistry C

ROYAL SOCIETY OF CHEMISTRY

PAPER

View Article Online
View Journal | View Issue

Cite this: J. Mater. Chem. C, 2025, 13, 17769

Inverting singlet–triplet gaps by design†

Lucas Rivera Blair and Tahereh Nematiaram *

Received 10th May 2025,
Accepted 23rd July 2025

DOI: 10.1039/d5tc01873k

rsc.li/materials-c

Inverted singlet–triplet (INVEST) emitters offer a promising path toward efficient, metal-free organic light-emitting diodes (OLEDs) by enabling exothermic reverse intersystem crossing. However, rational design of such materials remains elusive due to the complex interplay of structural and electronic factors. Here, we present a robust computational framework that screens 212 derivatives of phenalene, uthrene, and zethrene cores using a multi-tiered quantum chemical workflow (TD-DFT, SA-CASSCF, and SC-NEVPT2). We identify 15 novel INVEST molecules with negative singlet–triplet energy gaps and reveal generalisable design principles involving compact π-conjugation, heteroatom doping, and strategic fluorination. Crucially, solvent modeling confirms that INVEST behavior is retained across diverse environments, highlighting solution-processable potential. These findings advance the molecular design of metal-free triplet harvesters and offer a predictive toolkit for next-generation OLED materials.

1 Introduction

Organic light-emitting diodes have transformed modern display and lighting technologies due to their exceptional energy efficiency,[1,2] high contrast ratios,[3] and design flexibility.[4] However, their efficiency is fundamentally constrained by the spin-statistical distribution of excitons generated upon electrical excitation. Approximately 75% of these excitons reside in the triplet state (T_1), which is typically non-emissive in conventional fluorescent materials, limiting the internal quantum efficiency to a theoretical maximum of 25%.[5,6] This bottleneck necessitates the development of innovative strategies to harvest triplet excitons effectively and maximise OLED performance.

To overcome the limitations of triplet excitons in organic light-emitting materials, several strategies have been developed. One widely used approach involves phosphorescent emitters (PhOLEDs), which incorporate heavy-metal complexes (*e.g.*, Ir, Pt) to induce strong spin–orbit coupling, facilitating efficient intersystem crossing and enabling phosphorescence from the triplet state.[7–11] Although these materials achieve near-unity internal quantum efficiency, their reliance on rare and expensive metals presents challenges in terms of cost and sustainability. To circumvent the need for heavy metals, thermally activated delayed fluorescence (TADF) has been explored. TADF materials exploit a small singlet–triplet energy gap ($\Delta E_{S_1-T_1}$) to facilitate reverse intersystem crossing (RISC) from T_1 to the singlet excited state (S_1), allowing for delayed fluorescence.[12–14] This mechanism has enabled external quantum efficiencies exceeding 40%,[15] but TADF emitters often face trade-offs related to stability, efficiency roll-off, and color purity due to their reliance on charge-transfer states.[16]

Inverted singlet–triplet molecules have emerged as a promising new class of materials that defy Hunds rule by exhibiting a reversed energy ordering, wherein T_1 lies above S_1.[17–19] This inversion facilitates exothermic RISC, enabling rapid and thermally barrier-free triplet-to-singlet upconversion.[20] As such, INVEST molecules represent a compelling metal-free alternative to both PhOLEDs and TADF, with potential for enhanced efficiency and stability in OLED applications. Recent computational advances have significantly expanded the landscape of potential INVEST molecules. High-throughput virtual screening, combined with symmetry-based design strategies, has enabled the systematic exploration of vast chemical spaces, leading to the identification of a number of new candidates exhibiting inverted singlet–triplet energy gaps.[21–23] Despite this progress, many of the proposed structures remain closely related to triangulene motifs, which are already well-characterised in the context of singlet–triplet inversion.[24] Their behaviour is largely understood through established symmetry-derived design rules, such as those developed by Ricci *et al.*[25] More recently, attention has begun to shift toward more complex molecular frameworks. Compounds such as uthrene have been investigated, suggesting that extended conjugation and alternative topologies can also promote singlet–triplet inversion.[26] Additionally, some studies have explored structurally diverse, non-hydrocarbon systems including silapentafulvenes[27] and tetraatomic boron species[28] which under specific substitution patterns, also exhibit INVEST characteristics. Despite these developments, a comprehensive

Department of Pure and Applied Chemistry, University of Strathclyde, 295 Cathedral Street, Glasgow G1 1XL, UK. E-mail: tahereh.nematiaram@strath.ac.uk

† Electronic supplementary information (ESI) available. See DOI: https://doi.org/10.1039/d5tc01873k

understanding of how singlet–triplet inversion manifests across a broader range of molecular scaffolds remains limited.

In this study, we address this gap by systematically investigating three underexplored but chemically distinct scaffold families, phenalene, uthrene, and zethrene, as promising frameworks for singlet–triplet inversion. Unlike prior efforts that have largely focused on isolated examples or minor structural variations, our approach spans a broader design space by incorporating diverse substitution patterns, heteroatom doping strategies, and structural modifications across these cores. To this end, we implement a high-throughput, multi-tiered quantum chemical workflow to evaluate 212 functionalised derivatives. This approach allows us to uncover new INVEST candidates, assess how structural and electronic modifications influence inversion, and establish general design principles that extend beyond symmetry-based rules. Additionally, we evaluate the influence of solvent environments to gauge the robustness of INVEST behaviour under conditions relevant to device applications. This study aims to provide a deeper understanding of how molecular structure governs singlet–triplet inversion and to offer practical guidelines for the rational design of efficient, metal-free OLED emitters.

2 Computational workflow

To systematically identify and evaluate novel INVEST molecules, a rigorous computational approach was implemented, integrating geometry optimisation, singlet–triplet gap screening, high-level excited-state calculations, and solvent modelling, as summarised in Fig. 1. Similar multi-tiered workflows have been successfully applied in virtual screening studies[29–31] for various properties, including high-mobility materials,[32,33] singlet fission molecules,[34] TADF molecules,[13] transparent conductive materials,[35] and wide-band excitonic materials.[36] The workflow consists of the following stages:

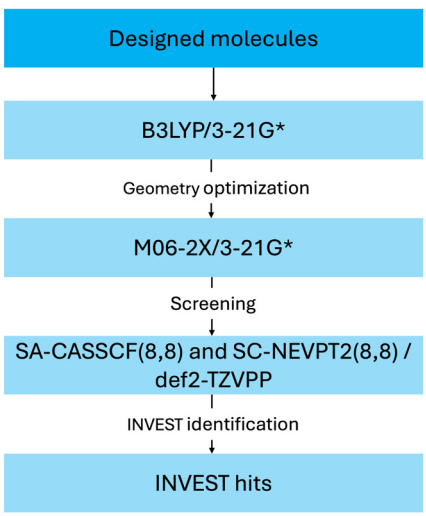

Fig. 1 Schematic representation of the computational workflow employed to identify and evaluate novel INVEST molecules. The workflow integrates geometry optimisation, pre-screening of singlet–triplet gaps using time-dependent density functional theory (TD-DFT) and high-level excited-state calculations (SA-CASSCF(8,8) and SC-NEVPT2(8,8)).

Initial structure selection and optimisation

The core structures of phenalene, uthrene, and zethrene were systematically modified to explore their electronic and structural properties. Substituents included electron-donating groups (NH_2, Me) and electron-withdrawing (NO_2, F) groups, heteroatoms (N, B, Si), and variations in aromatic ring size. Geometry optimizations were carried out using density functional theory (DFT) at the B3LYP/3-21G* level, selected for its well-established trade-off between computational efficiency and reasonable accuracy in modeling organic conjugated systems. All calculations employed the UltraFine integration grid to ensure numerical stability. The choice of B3LYP/3-21G* is further justified by ref. 23, which successfully applied the same level of theory in a high-throughput screening study of INVEST candidates. Vertical excitation energies (VEEs) were employed in place of adiabatic excitation energies (AEEs), based on prior studies of INVEST molecules which demonstrated minimal differences between the two approaches.[37] This assumption was further validated through a comparative analysis of VEE and AEE values for four representative compounds as summarised in Table S1 of the ESI.† The results confirmed that the use of VEEs reliably captured the inversion of the singlet–triplet energy gap.

Pre-screening of singlet–triplet gap

TD-DFT calculations were performed using the M06-2X functional in combination with the 3-21G* basis set to estimate the singlet–triplet energy gaps, following the approach outlined in ref. 23. This basis set was deliberately selected to enable efficient screening of large molecular libraries, balancing computational speed with the level of accuracy required to capture trends in excited-state energetics. Its use in high-throughput virtual screening has been validated in previous studies, where it demonstrated reliable performance across chemically diverse datasets.[23] To assess the suitability of this basis set in our context, we calculated $\Delta E_{S_1-T_1}$ for representative set of molecules using M06-2X/6-31G** and compared the results with those obtained using M06-2X/3-21G*. As shown in Table S2 (ESI†), the differences were minimal such that the largest deviation was only 0.037 eV, confirming that the smaller basis set offers sufficient accuracy for screening purposes, while enabling tractable computation across hundreds of compounds.

Molecules with singlet–triplet gaps smaller than 0.5 eV were shortlisted for further analysis. This threshold was chosen based on prior studies,[23,38] which demonstrate that a small or negative $\Delta E_{S_1-T_1}$ is critical for enabling efficient, exothermic reverse intersystem crossing. In contrast, a large positive gap renders RISC endothermic and kinetically unfavorable, severely limiting triplet harvesting. By applying this energetic cutoff, we ensure that only the most promising INVEST candidates are advanced to high-level multireference calculations.

High-level excited-state calculations

A subset of TD-DFT identified high-performance molecules was analysed with SA-CASSCF(8,8) and SC-NEVPT2(8,8) using the def2-TZVPP basis set. These calculations provided more accurate descriptions of excited-state energetics and electronic correlation effects, and are essential in confirming the singlet–triplet gap inversion predicted by TD-DFT. SA-CASSCF(8,8) was specifically employed to account for multi-configurational electronic states, while SC-NEVPT2(8,8) corrected dynamic correlation effects, leading to a more reliable estimation of $\Delta E_{S_1-T_1}$ values. The (8,8) active space was selected based on previous studies involving similar aromatic hydrocarbon frameworks, which demonstrated its adequacy for accurately describing electronic structures in such systems.[23,38] To further confirm the suitability of this choice, we compared $\Delta E_{S_1-T_1}$ values obtained with the (8,8) and larger (10,10) active spaces for four representative molecules (Table S3 in the ESI†). The results confirmed that the (8,8) active space reliably reproduced the singlet–triplet gap inversion, validating its use for this study. Notably, a molecule was classified as an INVEST candidate if either the SA-CASSCF(8,8) or SC-NEVPT2(8,8) calculation yielded a negative $\Delta E_{S_1-T_1}$, indicating inversion.

Solvent effects analysis

The influence of solvation on the singlet–triplet energy gap ($\Delta E_{S_1-T_1}$) was investigated using the conductor-like polarizable continuum model (CPCM)[39] applied to both SA-CASSCF(8,8) and SC-NEVPT2(8,8) computations. Solvent effects were evaluated in four solvents: toluene, acetonitrile, ethanol, and dichloromethane, which were selected to cover a wide range of dielectric constants and polarity characteristics. Toluene (ε = 2.38) represents a non-polar, weakly interacting environment;[40] acetonitrile (ε = 35.69) and ethanol (ε = 24.55) are highly polar solvents, probing strong solvation effects; while dichloromethane (ε = 8.93) serves as a moderately polar, intermediate case.[40] This selection allows for a comprehensive assessment of how solvent polarity influences INVEST behaviour. To test the accuracy of solvation modelling, calculated $\Delta E_{S_1-T_1}$ values for 1,2,3,5-tetrakis(carbazol-9-yl)-4,6-dicyanobenzene were compared across the four solvents, with experimental values reported in the literature.[41] These results are summarised in Table S4 of the ESI† and demonstrate that the chosen solvation model reasonably captures the solvent-dependent trends. All quantum chemical calculations are conducted using Gaussian16[42] for DFT and TD-DFT, and ORCA 6.0[43] for SA-CASSCF and SC-NEVPT2 calculations.

3 Results and discussions

Computational screening strategy

To identify INVEST candidates, we employed a rational computational screening approach centred on phenalene, uthrene, and zethrene (Fig. 2), as these structures exhibit tunable electronic properties,[44] making them ideal for investigating singlet–triplet energy inversion.

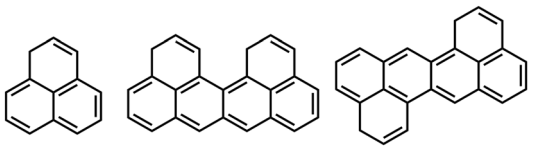

Fig. 2 The considered parent scaffolds (from left to right): phenalene, uthrene, and zethrene.

In order to systematically explore their potential for inversion, as shown in Fig. 3, we introduced three key molecular modifications: electron-donating (NH_2, Me) and electron-withdrawing (NO_2, F) groups, heteroatom substitutions (Si, B, N), and ring contractions and expansions. These modifications

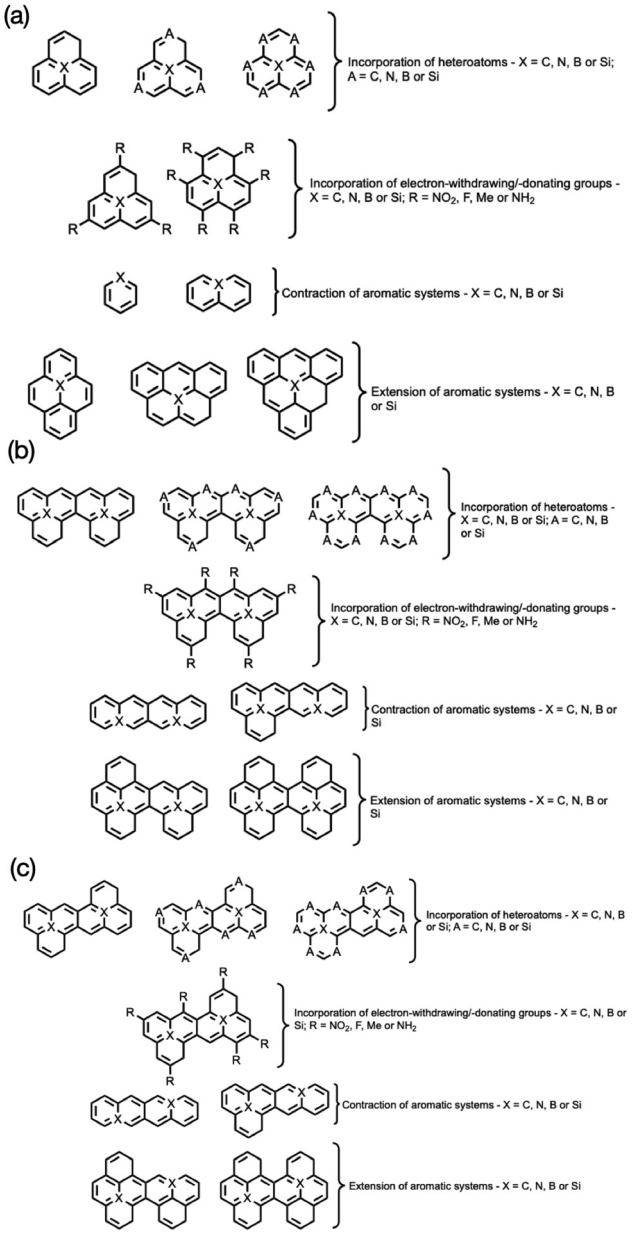

Fig. 3 Structural modifications of the (a) phenalene, (b) uthrene, and (c) zethrene scaffolds.

were applied to evaluate whether the parent scaffolds could be transformed into INVEST molecules by optimising their electronic structures for favourable inversion. For clarity, the molecules were classed as either C-, N-, Si- or B-centred, where the ''centre'' atom is labelled as X in Fig. 3. If a molecule has Con- or X- in the name (*e.g.*, Con-2N-U_a and X-N-phenalene), these refer to contraction or extension of the aromatic system, respectively. This systematic design yielded a total of 212 modified molecules (Fig. S1 of the ESI†), which were then screened using TD-DFT at M06-2X/3-21G* level of theory to estimate their singlet–triplet energy gap. Molecules with $\Delta E_{S_1-T_1} < 0.5$ eV were prioritised, as this threshold is necessary for efficient triplet-to-singlet upconversion.[23] This initial screening yielded 46 promising candidates, which were then subjected to high-level computational validation.

It is worth highlighting that the molecular modifications explored in this study can, in principle, give rise to a variety of structural isomers with differing thermodynamic stabilities. However, a comprehensive enumeration of all possible isomeric forms lies beyond the scope of this work. Instead, where applicable, we concentrated on substitution patterns that preserve molecular symmetry. This emphasis does not extend to systems involving ring contractions or extensions, where symmetry is inherently disrupted by design. Our decision to prioritise symmetry-preserving modifications is supported by numerous studies demonstrating that high molecular symmetry in polyaromatic hydrocarbons plays a critical role in enabling singlet–triplet inversion.[20,45–47] In particular, prior work on heteroatom substitution has shown that INVEST behaviour typically emerges only when the heteroatom is positioned at the molecular core.[48] To validate this symmetry-guided design principle, we analysed three positional isomers of N_3-B-phenalene (Fig. S2, ESI†). As summarised in Table S5 (ESI†), the most symmetric isomer, used as the representative structure in this study, was found to be both electronically favourable and thermodynamically stable. In contrast, the less symmetric isomers were higher in energy and less likely to exhibit INVEST behaviour. These findings underscore the dual importance of molecular symmetry in the design of INVEST-active compounds: symmetry not only promotes the electronic conditions necessary for singlet–triplet inversion but also contributes to the thermodynamic stability of the molecule. These insights provide a coherent and rational framework for the targeted development of future INVEST materials. Building on this foundation, future investigations that explore a broader spectrum of isomeric space, beyond symmetry-guided structures, may further elucidate the structure–property relationships that underpin effective INVEST design.

High-level validation & INVEST confirmation

To ensure the accuracy of the TD-DFT results, the 46 shortlisted molecules underwent further analysis using SA-CASSCF(8,8) and SC-NEVPT2(8,8) with the def2-TZVPP basis set. These high-level methods provide a more accurate description of electronic correlation effects, improving the reliability of singlet–triplet energy predictions.[49] Fig. 4(a) illustrates the

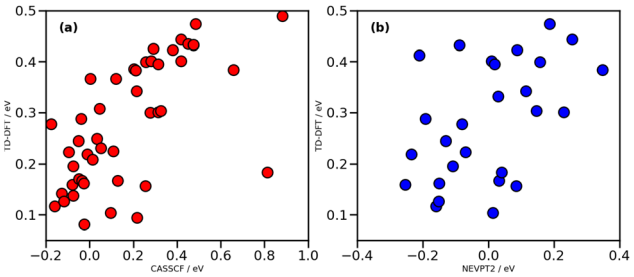

Fig. 4 Comparison of TD-DFT with (a) SA-CASSCF(8,8) and (b) SC-NEVPT2(8,8) singlet–triplet energy gaps in the gas phase.

correlation between the singlet–triplet energy gap, $\Delta E_{S_1-T_1}$, computed using TD-DFT and CASSCF. A general positive correlation is observed, indicating that as CASSCF values increase, TD-DFT values tend to increase as well. However, the noticeable spread of data points suggests significant deviations, implying that while TD-DFT follows a similar trend, it does not always quantitatively match CASSCF results. Similarly, Fig. 4(b) compares TD-DFT with NEVPT2, a second-order perturbation theory method built upon CASSCF. The weaker correlation in this case suggests that TD-DFT does not reliably reproduce NEVPT2 trends, likely due to missing dynamic correlation effects. These findings highlight the varying agreement between TD-DFT and multireference methods, emphasising the need for caution when applying TD-DFT to systems where strong electron correlation effects are significant.

Following high-level validation, 15 molecules were confirmed as genuine INVEST candidates based on SA-CASSCF(8,8) and SC-NEVPT2(8,8) calculations, each exhibiting a negative singlet–triplet energy gap ($\Delta E_{S_1-T_1}$) (Fig. 5). The optimized geometries of these molecules, along with details of the orbitals included in the active space, are provided in the ESI.† These results, summarised in Table 1, were compared against initial TD-DFT predictions,

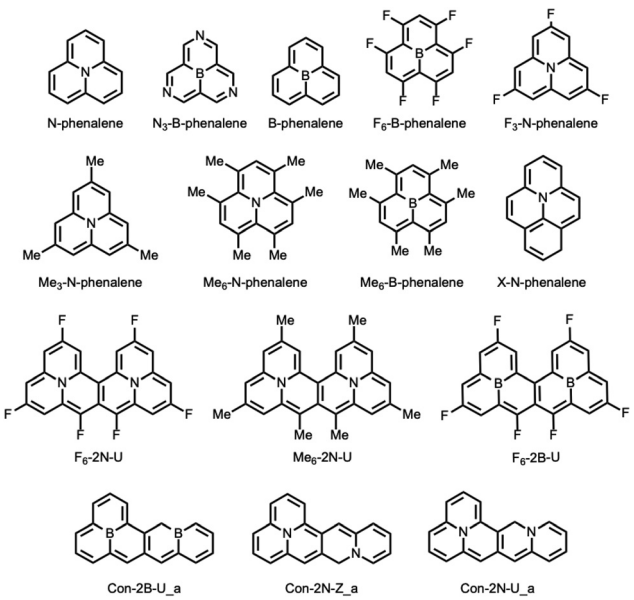

Fig. 5 Molecular structures of the 15 identified INVEST candidates.

Table 1 Comparison of $\Delta E_{S_1-T_1}$ values for INVEST molecules calculated using TD-DFT, SA-CASSCF(8,8) (denoted as CASSCF), and SC-NEVPT2(8,8) (denoted as NEVPT2). Italicised entries are included for reference. All values are reported in eV

Molecules	$\Delta E_{S_1-T_1}^{TD\text{-}DFT}$	$\Delta E_{S_1-T_1}^{CASSCF}$	$\Delta E_{S_1-T_1}^{NEVPT2}$
Phenalene	*1.499*	*2.331*	—
Uthrene	*1.323*	*2.394*	—
Zethrene	*1.340*	*1.935*	—
Me_6-2N-U	0.278	−0.175	−0.080
F_3-N-phenalene	0.116	−0.159	−0.160
Con-2N-U_a	0.142	−0.128	—
Me_6-B-phenalene	0.126	−0.117	−0.151
Con-2N-Z_a	0.223	−0.096	−0.070
B-phenalene	0.138	−0.075	—
X-N-phenalene	0.195	−0.075	−0.108
F_6-2B-U	0.244	−0.052	−0.130
Me_3-N-phenalene	0.170	−0.050	—
F_6-2N-U	0.288	−0.039	−0.192
Me_6-N-phenalene	0.167	−0.035	—
N-Phenalene	0.161	−0.026	−0.150
N_3-B-phenalene	0.081	−0.024	—
Con-2B-U_a	0.219	−0.011	−0.235
F_6-B-phenalene	0.159	−0.080	−0.254

alongside benchmark reference compounds. While TD-DFT proved useful for initial screening, it consistently overestimated the singlet–triplet gap and failed to detect inversion in any of the confirmed candidates. In contrast, both CASSCF and NEVPT2 reliably predicted negative gaps, validating the presence of singlet–triplet inversion. In most cases, NEVPT2 yielded more negative values than CASSCF, reflecting its more complete treatment of dynamic electron correlation. However, as shown in Fig. 6, this trend was not universal. Although many NEVPT2 values were lower than their CASSCF counterparts, the relationship was not strictly linear, and in some instances, NEVPT2 produced less negative values. This indicates that the magnitude of NEVPT2 corrections does not scale uniformly with CASSCF predictions. A small subset of cases evaluated using a larger (10,10) active space (Table S3, ESI†) even showed the opposite trend more prominently, with NEVPT2 yielding less negative gaps than CASSCF. However, given the limited size of this dataset, these results are likely anomalous. Additionally, several NEVPT2 calculations failed to converge, highlighting known challenges associated with multireference perturbation theory in complex systems.

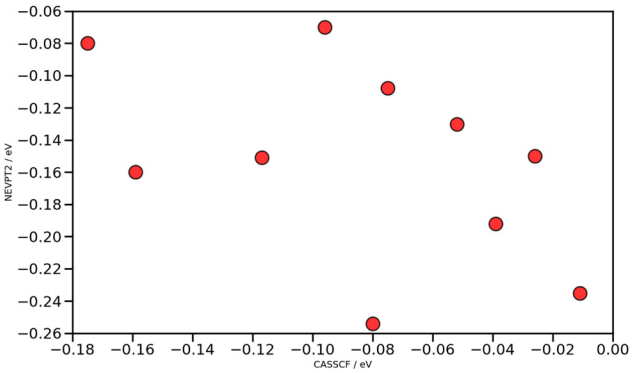

Fig. 6 Comparison of SA-CASSCF(8,8) and SC-NEVPT2(8,8) results.

Despite these challenges, the agreement between CASSCF and NEVPT2 in the majority of cases confirms the robustness of our validation protocol and underscores the necessity of multireference methods for accurately characterising INVEST behaviour.

Considering the 15 identified INVEST molecules, a clear structural trend emerged from our analysis: phenalene-based derivatives consistently exhibited stronger INVEST behaviour than their uthrene and zethrene counterparts, likely due to the distinct electronic features of the phenalene core. As noted by Pollice *et al.*,[37] phenalene-type molecules typically show weak HOMO–LUMO spatial overlap, which contributes to small or inverted singlet–triplet energy gaps. This reduced overlap weakens the exchange interaction, lowering the T_1 energy to a lesser extent than the S_1, thereby facilitating gap inversion. Additionally, the S_1 state often possesses substantial double-excitation character, leading to further stabilisation *via* spin-polarisation effects. Collectively, these factors create an electronic environment that favours INVEST behaviour, explaining the consistent inversions observed in phenalene-based systems.

With 15 molecules confirmed as true INVEST candidates, a natural next consideration is their experimental viability. To assess this, we evaluated the synthetic accessibility of the selected molecules using the Synthetic Accessibility Score (SAScore), a cheminformatics tool developed by Ertl and Schuffenhauer.[50] The SAScore estimates synthetic ease by combining fragment contributions with penalties for structural complexity, such as unusual substructures, stereocenters, and large ring systems. Values typically range from 1 (very easy to synthesise) to 10 (very difficult). The calculated scores for our INVEST candidates, summarised in Table 2, fall between 2.672 and 5.323, which indicates a generally moderate level of synthetic accessibility.[51]

This suggests that many of the compounds are not only promising from a computational perspective but may also be feasible to synthesise using standard laboratory techniques. Among the candidates, N-phenalene is especially promising. It corresponds to the known structure pyrido[2,1,6-*de*]quinolizine, which has been previously explored in medicinal chemistry. Accordingly, derivatives of N-phenalene are likely to be

Table 2 The SAScore of INVEST hits

Molecules	SAScore
Me_6-2N-U	2.672
F_3-N-phenalene	4.251
Con-2N-U_a	4.664
Me_6-B-phenalene	4.186
Con-2N-Z_a	4.681
B-phenalene	4.791
X-N-phenalene	4.213
F_6-2B-U	5.199
Me_3-N-phenalene	3.973
F_6-2N-U	2.865
Me_6-N-phenalene	3.682
N-phenalene	3.921
N_3-B-phenalene	5.323
Con-2B-U_a	—
F_6-B-phenalene	4.596

more feasible to be synthesized. In contrast, uthrene remains a hypothetical compound, with no successful synthesis reported to date.[52] Any attempt to prepare its derivatives would therefore require the prior synthesis and full characterization of the parent structure, which presents an experimental challenge. As evident from Table 2, the SAScore for Con-2B-U_a could not be computed. This typically occurs when the molecule's structure cannot be parsed correctly by the scoring algorithm, often due to unusual or highly complex features. Overall, this analysis identifies a subset of INVEST candidates that not only exhibit strong theoretical promise but also possess realistic synthetic feasibility, thereby helping to bridge the gap between computational discovery and experimental implementation.

Impact of structural modifications on INVEST behaviour

The effectiveness of inverted singlet–triplet emitters is expected to be governed by their electronic structure, which can be systematically tuned through chemical modifications such as electron-donating and electron-withdrawing substituents, heteroatom doping, and structural adjustments of the conjugated core. To analyse these effects, we computed and visualised the frontier molecular orbitals (FMOs) of INVEST molecules (Fig. S3 and S4, ESI†) and representative examples are shown in Fig. 7. Below, we discuss how each modification influences the singlet–triplet energy gap.

Electron-donating groups, such as amino (–NH_2) substituents, are generally known to raise the energy of the HOMO.[53] However, this effect alone does not necessarily result in a reduced singlet–triplet energy gap ($\Delta E_{S_1-T_1}$). For instance, in the molecule $(NH_2)_6$-2B-U (Fig. 7(a)), both the HOMO (left) and the LUMO (right) remain largely delocalised across the π-system, with significant contributions from the conjugated core. This delocalisation indicates that the amino groups do not induce a meaningful spatial separation between the frontier orbitals, a critical factor for achieving efficient singlet–triplet inversion.[25] In the absence of substantial orbital localisation, the exchange interaction remains relatively strong, thereby limiting any potential reduction in $\Delta E_{S_1-T_1}$. Computational results further support this conclusion, demonstrating that even strong electron-donating substituents, on their own, are insufficient to enable inversion.

Electron-withdrawing substituents, such as fluorine (–F), can stabilise the LUMO and, under appropriate conditions, contribute to a reduction in the singlet–triplet energy gap ($\Delta E_{S_1-T_1}$). The molecule F_3-N-phenalene (Fig. 7(b)) illustrates this effect: while both the HOMO and LUMO remain broadly delocalised, the LUMO exhibits increased electron density near the fluorinated region, indicating localised stabilisation. This modulation of the electronic structure can promote singlet–triplet inversion, as reflected in the significantly negative computed $\Delta E_{S_1-T_1}$ value (−0.159 eV, SA-CASSCF). This observation is consistent with previous studies showing that fluorine substitution can enhance charge-transfer character by modulating orbital energies and distributions, which in some cases contributes to reduced singlet–triplet energy gaps.[54] This finding also aligns with previous studies demonstrating that electron-withdrawing substituents, including phosphonium groups, can reduce the singlet–triplet energy gap, as observed in osmapyridinium complexes.[55]

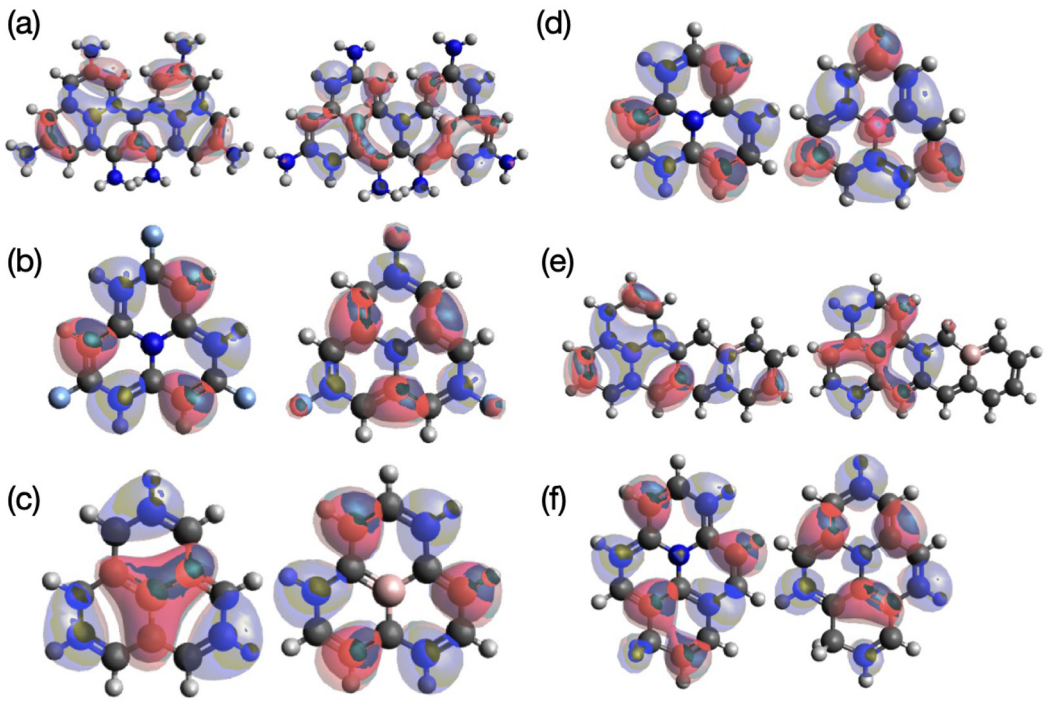

Fig. 7 Molecular orbitals of selected INVEST molecules. In all panels, the left side represents the HOMO, and the right side represents the LUMO. (a) $(NH_2)_6$-2B-U, (b) F_3-N-phenalene, (c) B-phenalene, (d) N-phenalene, (e) Con-2B-U_a, (f) X-N-phenalene.

Heteroatom doping, particularly with boron (B) and nitrogen (N), effectively modulates orbital energies and influences the singlet–triplet energy gap. The B-phenalene system (Fig. 7(c)) exemplifies the impact of boron incorporation: the LUMO shows a moderate degree of localisation around the boron atom, whereas the HOMO remains more uniformly delocalised over the conjugated framework. This resulting electronic asymmetry reduces the electron density overlap between the frontier orbitals, thereby lowering the exchange interaction and supporting the stabilisation of inverted singlet–triplet ordering. The computed $\Delta E_{S_1-T_1}$ value (−0.075 eV, SA-CASSCF) confirms that boron substitution is effective in facilitating singlet–triplet inversion. Similarly, in N-phenalene (Fig. 7(d)), nitrogen doping leads to some degree of localisation of the HOMO around the nitrogen atoms, while the LUMO remains relatively delocalised across the conjugated framework. This asymmetry in orbital distribution reduces the spatial overlap between the frontier orbitals, thereby lowering the exchange interaction and resulting in a slightly negative singlet–triplet energy gap (−0.026 eV, SA-CASSCF). Compared to boron, which primarily stabilises and localises the LUMO, nitrogen induces localisation mainly in the HOMO. As a result, its overall effect on singlet–triplet inversion is more modest.

Geometric structure plays a pivotal role in modulating frontier molecular orbital distribution and thus influencing singlet–triplet inversion. In the contracted uthrene derivative Con-2B-U_a (Fig. 7(e)), the HOMO remains highly delocalised across the π-system, while the LUMO exhibits partial localisation in specific molecular regions. This moderate LUMO localisation reduces spatial overlap between the frontier orbitals, thereby weakening the exchange interaction and enabling singlet–triplet inversion. The calculated $\Delta E_{S_1-T_1}$ of −0.011 eV (SA-CASSCF) confirms this behaviour. These results suggest that controlled ring contraction can promote inversion by enhancing orbital asymmetry while maintaining sufficient delocalisation for electronic coupling. Conversely, expansion of the conjugated system can increase spatial separation between the HOMO and LUMO, further reducing orbital overlap and suppressing the singlet–triplet exchange interaction. This effect is exemplified by the X-N-phenalene molecule (Fig. 7(f)), where the HOMO and LUMO are localised in distinct molecular regions. The resulting negative $\Delta E_{S_1-T_1}$ of −0.075 eV confirms effective singlet–triplet inversion.

Beyond the S_1–T_1 gap, higher excited states may also contribute to spin-conversion dynamics in INVEST molecules, particularly when the energy difference between the second singlet and triplet states ($\Delta E_{S_2-T_2}$) is small. Under such conditions, reverse intersystem crossing from T_2 to S_2 has been proposed as an alternative upconversion pathway, especially when internal conversion to T_1 is inefficient or slower.[38] This mechanism becomes especially relevant when S_2 and T_2 are nearly degenerate or inverted, potentially enabling $T_2 \rightarrow S_2 \rightarrow S_1$ transitions. To evaluate the accessibility of this pathway in our INVEST candidates, we examined how chemical substitution affects ΔE_{S2-T2} across phenalene, uthrene, and zethrene derivatives (Table 3). A more detailed version of this table, including the singlet and triplet energies, can be found in Table S6 (ESI†). Our analysis reveals that in 14 of the 15 INVEST derivatives, $\Delta E_{S_2-T_2}$ decreases relative to the corresponding parent scaffolds, indicating enhanced proximity of the S_2 and T_2 states. This effect is particularly pronounced in the uthrene derivatives, where all substitutions led to lower energy gaps. Among these, Me_6-2N-U, F_6-2N-U, and F_6-2B-U display negative $\Delta E_{S_2-T_2}$ values (either at CASSCF or NEVPT2 levels), suggesting a potential inversion. However, structural contraction of the aromatic uthrene system (*e.g.*, Con-2B-U_a) did not significantly affect $\Delta E_{S_2-T_2}$. Phenalene derivatives generally showed more modest reductions in $\Delta E_{S_2-T_2}$ upon substitution. A notable exception is N_3-B-phenalene, where the gap decreased dramatically by 1.313 eV. This large reduction can be attributed to heteroatom-induced orbital asymmetry, which disrupts HOMO–LUMO overlap and affects the energetic positioning of higher excited states. Zethrene derivatives followed similar trends, though Con-2N-Z_a displayed an anomalous increase in $\Delta E_{S_2-T_2}$ by 0.195 eV due to a greater destabilisation of S_2 compared to T_2. These findings suggest that chemical modifications not only tune the S_1–T_1 gap but also can influence higher excited state energetics in a scaffold-dependent manner.

Table 3 Comparison of $\Delta E_{S_2-T_2}$ values for INVEST molecules calculated using SA-CASSCF(8,8), and SC-NEVPT2(8,8). All values are reported in eV. In the fluorinated compounds, this arises from stabilisation of the LUMO, whereas in the methylated analogue, the HOMO is destabilised due to electron-donating effects

Molecules	$\Delta E^{CASSCF}_{S_2-T_2}$	$\Delta E^{NEVPT2}_{S_2-T_2}$
Phenalene	*1.693*	—
Uthrene	*0.729*	—
Zethrene	*0.730*	—
Me_6-2N-U	−0.084	−0.053
F_3-N-phenalene	1.198	0.909
Con-2N-U_a	0.686	—
Me_6-B-phenalene	1.277	1.064
Con-2N-Z_a	0.925	0.765
B-phenalene	1.363	—
X-N-phenalene	1.242	1.018
F_6-2B-U	−0.001	−0.074
Me_3-N-phenalene	1.253	—
F_6-2N-U	0.059	−0.131
Me_6-N-phenalene	1.236	—
N-phenalene	1.240	1.085
N_3-B-phenalene	0.380	—
Con-2B-U_a	0.714	0.700
F_6-B-phenalene	1.391	0.895

Solvent effects on singlet–triplet energy gap

Understanding the influence of environmental factors is essential for translating molecular design into device performance.[56] We, therefore, investigate how solvents with varying dielectric properties affect the singlet–triplet energy gap in INVEST candidates. The impact of solvent on the singlet–triplet energy gap of the investigated molecules was found to be generally weak, with only minor variations observed across different dielectric environments. While solvation can potentially influence excited-state energetics by modifying charge distribution and orbital stabilisation,[57] no systematic correlation was

Table 4 Comparison of $\Delta E_{S_1-T_1}$ values of INVEST molecules in the gas-phase and solvents calculated with SA-CASSCF(8,8); all values are in eV

Molecules	Gas-phase	Acetonitrile	Ethanol	Dichloromethane	Toluene
Me_6-2N-U	−0.175	−0.173	−0.169	−0.169	−0.170
F_3-N-phenalene	−0.159	−0.068	−0.144	−0.144	−0.139
Con-2N-U_a	−0.128	−0.126	−0.120	−0.126	−0.164
Me_6-B-phenalene	−0.117	−0.103	−0.090	−0.091	−0.094
Con-2N-Z_a	−0.096	−0.098	−0.103	−0.103	−0.101
B-phenalene	−0.075	−0.083	—	−0.091	−0.036
X-N-phenalene	−0.075	−0.072	—	−0.055	—
F_6-2B-U	−0.052	−0.065	−0.074	−0.074	−0.072
Me_3-N-phenalene	−0.050	−0.043	−0.041	−0.049	−0.043
F_6-2N-U	−0.039	−0.151	—	—	—
Me_6-N-phenalene	−0.035	−0.023	—	—	−0.029
N-phenalene	−0.026	−0.028	−0.027	−0.027	−0.027
N_3-B-phenalene	−0.024	—	—	—	—
Con-2B-U_a	−0.011	−0.007	−0.042	—	−0.083
F_6-B-phenalene	−0.080	−0.073	−0.069	−0.075	−0.071

established between solvent polarity and the magnitude or direction of $\Delta E_{S_1-T_1}$ shifts. This suggests that while solvents introduce local perturbations, they do not override the intrinsic electronic structure factors governing singlet–triplet inversion in these molecules.

A closer examination of specific molecules reveals that solvation effects manifest differently depending on the electronic structure and the nature of solvent interactions, as shown in Table 4. In Con-2B-U_a, the singlet–triplet energy gap exhibited a significant decrease in toluene compared to the gas phase, compared to solvent-induced shifts in the remaining molecules, shifting from $\Delta E_{S_1-T_1}^{\text{gas-phase}} = -0.011$ eV to $\Delta E_{S_1-T_1}^{\text{toluene}} = -0.083$ eV. This pronounced decrease suggests that toluene preferentially stabilises the singlet excited state (S_1) relative to the triplet state (T_1), thereby enhancing the negative $\Delta E_{S_1-T_1}$. In contrast, Me_6-B-phenalene displayed an opposing trend, where $\Delta E_{S_1-T_1}$ increased slightly in acetonitrile, shifting from $\Delta E_{S_1-T_1}^{\text{gas-phase}} = -0.117$ eV to $\Delta E_{S_1-T_1}^{\text{acetonitrile}} = -0.083$ eV. This behaviour suggests that acetonitrile stabilises the T_1 state more effectively than the S_1 state, possibly due to stronger dipolar interactions with charge-separated excitonic states. Similarly, Con-2N-U_a exhibited a solvent-induced reduction in $\Delta E_{S_1-T_1}$ when moving from the gas phase ($\Delta E_{S_1-T_1}$ = −0.128 eV) to toluene ($\Delta E_{S_1-T_1}$ = −0.164 eV), reinforcing the observation that compact molecular frameworks can be more sensitive to solvation effects.

Despite these solvent-induced variations, the fundamental INVEST property, where the singlet state remains energetically lower than the triplet, was consistently preserved, reinforcing that solvation effects are secondary in determining the electronic ordering of these states. The solvation-induced shift in $\Delta E_{S_1-T_1}$ can be quantified as $\Delta\Delta E_{S_1-T_1} = \Delta E_{S_1-T_1}^{\text{solvent}} - \Delta E_{S_1-T_1}^{\text{gas-phase}}$. Analysis across all solvents revealed that most molecules exhibited $\Delta\Delta E_{S_1-T_1}$ shifts below 0.1 eV, indicating that solvation effects are subtle and do not induce significant reordering of the singlet–triplet levels. However, the degree of sensitivity to solvent varied based on structural features, particularly in molecules with contracted aromatic systems. For example, Con-2B-U_a, which contains boron, a highly electron-deficient element, demonstrated the strongest solvent dependence. Boron substitution increases local charge density asymmetry, making the molecule more susceptible to solvent-induced polarisation effects. Similarly, in Con-2N-U_a, nitrogen incorporation contributed to a reduced $\Delta E_{S_1-T_1}$ upon solvation in toluene, further supporting the idea that electronic asymmetry enhances solvent sensitivity.

The structural rigidity of the aromatic system also played a key role in determining solvent influence. Molecules with more flexible frameworks exhibited weaker solvent dependence, while contracted systems, such as those with fused boron or nitrogen centres, showed enhanced solvent sensitivity. The solvation effect in these molecules is thus governed by a delicate interplay between electronic polarisation, orbital interactions, and the intrinsic rigidity of the molecular scaffold.

While solvent effects observed in solution-phase calculations offer valuable insights, their relevance to real-world applications, such as solution-processed OLED fabrication, requires careful consideration. In thin-film device environments, molecules are subject to additional perturbations from molecular packing, intermolecular interactions, and dielectric screening, all of which can further influence excited-state energetics.[58] The relatively small shifts in $\Delta E_{S_1-T_1}$ observed in solution suggest that similar perturbations may occur in the solid state, potentially affecting the efficiency of reverse intersystem crossing and the overall performance of OLEDs. Nevertheless, when compared to the differences arising from methodological choices such as using CASSCF *versus* NEVPT2, expanding the active space, or employing adiabatic rather than vertical excitation energies, the impact of solvation effects, although theoretically interesting, is unlikely to significantly influence real-world device performance. Future studies should still extend this analysis to the solid state, as solvent models do not fully capture the complexity of condensed-phase environments.

Oscillator strength considerations

Achieving inverted singlet–triplet energy gaps ($\Delta E_{S_1-T_1} < 0$) often comes at the cost of reduced radiative efficiency. This

trade-off arises because the orbital characteristics that promote inversion, namely, reduced HOMO–LUMO spatial overlap and multiconfigurational singlet states, tend to suppress the transition dipole moment, resulting in low oscillator strengths (f) for the $S_1 \rightarrow S_0$ transition. This limitation is well documented in the literature and represents a key challenge in the design of practical INVEST emitters.[23,59–61] Our results support this general trend. As shown in Table S7 (ESI†), the oscillator strengths of the investigated INVEST molecules, calculated at the SA-CASSCF(8,8) level, are consistently low. Most values fall in the range of 10^{-4} to 10^{-3}, with molecules such as F_6-2B-U (f = 0.0025) and Con-2B-U_a (f = 0.0042) demonstrating the highest radiative potential. Importantly, these values are not negligible: similar oscillator strengths have been reported for previously studied INVEST systems,[60,61] supporting their potential suitability for further development as functional emitters. Moreover, several molecules exhibit solvent-dependent changes in oscillator strength, suggesting that radiative properties can be modulated through external environmental factors. For instance, the oscillator strength of F_3-N-phenalene increases from f = 0.0003 in the gas phase to f = 0.0007 in dichloromethane, while Con-2N-Z_a reaches f = 0.0032 in multiple polar solvents (acetonitrile, ethanol, and dichloromethane), compared to just f = 0.0010 in the gas phase. Conversely, Con-2B-U_a displays a decrease in f across solvents, from f = 0.0042 in the gas phase to f = 0.0015 and 0.0009 in dichloromethane and toluene, respectively. These variations highlight the role of solvent polarity and solute–solvent interactions in tuning transition dipole moments, a feature that could be leveraged through host matrix or device engineering.

While enhancing oscillator strength was not the central goal of this study, our findings underscore that radiative properties are tunable and can be systematically improved in future work. Design strategies known to enhance f, such as structural rigidification, symmetry breaking, and donor–acceptor tuning, have been widely applied in organic photophysics and are fully compatible with the INVEST design framework established here.[61] Applying these modifications to the scaffolds identified in this study offers a promising path toward developing high-performance inverted emitters with improved radiative efficiency.

4 Conclusions

This study presents a comprehensive computational strategy for the rational design of inverted singlet–triplet emitters, promising candidates for next-generation, metal-free OLED materials. By screening 212 functionalised derivatives across three core scaffolds (phenalene, uthrene, and zethrene) and applying a multi-level quantum chemical workflow, we identified 15 molecules that exhibit robust singlet–triplet inversion. Our results reveal transferable design principles: compact conjugated frameworks, targeted boron or nitrogen doping, and moderate fluorination synergistically promote energy gap inversion. Notably, INVEST behaviour is maintained across a range of dielectric environments, demonstrating the relevance of these emitters for solution-processable applications. Although oscillator strengths remain modest, several structures combine singlet–triplet inversion with non-negligible radiative potential, offering a path forward for optimising brightness without sacrificing energy efficiency. Overall, our findings deliver general design rules and validated molecular candidates that advance the discovery of sustainable, heavy-metal-free OLED materials. This framework can potentially accelerate future development of efficient triplet-harvesting emitters with improved performance and environmental compatibility.

Conflicts of interest

There are no conflicts to declare.

Data availability

All data supporting the findings of this study are provided in the ESI† and are publicly accessible *via* the following GitHub repository: **https://github.com/aram-tahereh-git/INVEST_Paper_JMCC**.

Notes and references

1 R. Pode, *Renewable Sustainable Energy Rev.*, 2020, **133**, 110043.
2 M. Vasilopoulou, A. R. b Mohd Yusoff, M. Daboczi, J. Conforto, A. E. X. Gavim, W. J. da Silva, A. G. Macedo, A. Soultati, G. Pistolis, F. K. Schneider, Y. Dong, P. Jacoutot, G. Rotas, J. Jang, G. C. Vougioukalakis, C. L. Chochos, J.-S. Kim and N. Gasparini, *Nat. Commun.*, 2021, **12**, 4868.
3 R. Singh, K. N. Unni and A. Solanki, *et al.*, *Opt. Mater.*, 2012, **34**, 716–723.
4 S.-J. Zou, Y. Shen, F.-M. Xie, J.-D. Chen, Y.-Q. Li and J.-X. Tang, *Mater. Chem. Front.*, 2020, **4**, 788–820.
5 M. A. Baldo, D. F. OBrien, M. E. Thompson and S. R. Forrest, *Phys. Rev. B: Condens. Matter Mater. Phys.*, 1999, **60**, 14422–14428.
6 M. A. Baldo, M. E. Thompson and S. R. Forrest, *Nature*, 2000, **403**, 750–753.
7 S. Arunkumar, D. Ghosh and G. R. Kumar, *Results Chem.*, 2022, **4**, 100399.
8 J.-S. Huh, M. J. Sung, S.-K. Kwon, Y.-H. Kim and J.-J. Kim, *Adv. Funct. Mater.*, 2021, **31**, 2100967.
9 H. J. Park, J.-H. Jang, J.-H. Lee and D.-H. Hwang, *ACS Appl. Mater. Interfaces*, 2022, **14**, 34901–34908.
10 T. Fleetham, G. Li and J. Li, *ACS Appl. Mater. Interfaces*, 2015, **7**, 16240–16246.
11 S. Lamansky, P. Djurovich, D. Murphy, F. Abdel-Razzaq, H.-E. Lee, C. Adachi, P. E. Burrows, S. R. Forrest and M. E. Thompson, *J. Am. Chem. Soc.*, 2001, **123**, 4304–4312.
12 S. Boudin, *J. Chim. Phys*, 1930, **27**, 285–290.
13 K. Zhao, Ö. H. Omar, T. Nematiaram, D. Padula and A. Troisi, *J. Mater. Chem. C*, 2021, **9**, 3324–3333.
14 S. M. Pratik, V. Coropceanu and J.-L. Bredas, *Chem. Mater.*, 2022, **34**, 8022–8030.

15 K. R. Naveen, H. Lee, R. Braveenth, D. Karthik, K. J. Yang, S. J. Hwang and J. H. Kwon, *Adv. Funct. Mater.*, 2022, **32**, 2110356.
16 D. Y. Kondakov, *Philos. Trans. R. Soc., A*, 2015, **373**, 20140321.
17 N. Aizawa, Y.-J. Pu, Y. Harabuchi, A. Nihonyanagi, R. Ibuka, H. Inuzuka, B. Dhara, Y. Koyama, K.-I. Nakayama, S. Maeda, F. Araoka and D. Miyajima, *Nature*, 2022, **609**, 502–506.
18 M. H. Garner, J. T. Blaskovits and C. Corminboeuf, *Chem. Sci.*, 2023, **14**, 10458–10466.
19 T. Sato, M. Uejima, K. Tanaka, H. Kaji and C. Adachi, *J. Mater. Chem. C*, 2015, **3**, 870–878.
20 D. Valverde, C. T. Ser, G. Ricci, K. Jorner, R. Pollice, A. Aspuru-Guzik and Y. Olivier, *ACS Appl. Mater. Interfaces*, 2024, **16**, 66991–67001.
21 R. Pollice, B. Ding and A. Aspuru-Guzik, *Matter*, 2024, **7**, 1161–1186.
22 J. Terence Blaskovits, M. H. Garner and C. Corminboeuf, *Angew. Chem., Int. Ed.*, 2023, **62**, e202218156.
23 O. H. Omar, X. Xie, A. Troisi and D. Padula, *J. Am. Chem. Soc.*, 2023, **145**, 19790–19799.
24 J. Sanz-Rodrigo, G. Ricci, Y. Olivier and J.-C. Sancho-Garcia, *J. Phys. Chem. A*, 2021, **125**, 513–522.
25 G. Ricci, J.-C. Sancho-García and Y. Olivier, *J. Mater. Chem. C*, 2022, **10**, 12680–12698.
26 M. H. Garner, J. T. Blaskovits and C. Corminboeuf, *Chem. Commun.*, 2024, **60**, 2070–2073.
27 J. Wu, A. M. Rouf, Y. Huang, D. Zhuang and J. Zhu, *Phys. Chem. Chem. Phys.*, 2020, **22**, 4668–4676.
28 C. Dai, Y. Huang and J. Zhu, *Organometallics*, 2020, **39**, 2602–2608.
29 E. O. Pyzer-Knapp, C. Suh, R. Gómez-Bombarelli, J. Aguilera-Iparraguirre and A. Aspuru-Guzik, *Annu. Rev. Mater. Res.*, 2015, **45**, 195–216.
30 Ö. H. Omar, M. Del Cueto, T. Nematiaram and A. Troisi, *J. Mater. Chem. C*, 2021, **9**, 13557–13583.
31 Ö. H. Omar, T. Nematiaram, A. Troisi and D. Padula, *Sci. Data*, 2022, **9**, 54.
32 T. Nematiaram, D. Padula, A. Landi and A. Troisi, *Adv. Funct. Mater.*, 2020, **30**, 2001906.
33 T. Nematiaram and A. Troisi, *Mater. Horiz.*, 2020, **7**, 2922–2928.
34 D. Padula, Ö. H. Omar, T. Nematiaram and A. Troisi, *Energy Environ. Sci.*, 2019, **12**, 2412–2416.
35 T. Nematiaram and A. Troisi, *Chem. Mater.*, 2022, **34**, 4050–4061.
36 T. Nematiaram, D. Padula and A. Troisi, *Chem. Mater.*, 2021, **33**, 3368–3378.
37 R. Pollice, P. Friederich, C. Lavigne, G. dos Passos Gomes and A. Aspuru-Guzik, *Matter*, 2021, **4**, 1654–1682.
38 G. Ricci, A. Landi, J. C. Sancho Garcia and Y. Olivier, Enhancing Reverse Intersystem Crossing with Extended Inverted Singlet–Triplet (XINVEST) systems, 2024, **https://chemrxiv.org/engage/chemrxiv/article-details/6704d4dacec5d6c1428f2e99**.
39 S. Samavat, R. Ghiasi and B. Mohtat, *Inorg. Chem. Res.*, 2021, **5**, 257–264.
40 C. Reichardt and T. Welton, *Solvents and Solvent Effects in Organic Chemistry*, Wiley, 1st edn, 2010.
41 R. Ishimatsu, S. Matsunami, K. Shizu, C. Adachi, K. Nakano and T. Imato, *J. Phys. Chem. A*, 2013, **117**, 5607–5612.
42 M. J. Frisch, G. W. Trucks, H. B. Schlegel, G. E. Scuseria, M. A. Robb, J. R. Cheeseman, G. Scalmani, V. Barone, G. A. Petersson, H. Nakatsuji, X. Li, M. Caricato, A. V. Marenich, J. Bloino, B. G. Janesko, R. Gomperts, B. Mennucci, H. P. Hratchian, J. V. Ortiz, A. F. Izmaylov, J. L. Sonnenberg, D. Williams-Young, F. Ding, F. Lipparini, F. Egidi, J. Goings, B. Peng, A. Petrone, T. Henderson, D. Ranasinghe, V. G. Zakrzewski, J. Gao, N. Rega, G. Zheng, W. Liang, M. Hada, M. Ehara, K. Toyota, R. Fukuda, J. Hasegawa, M. Ishida, T. Nakajima, Y. Honda, O. Kitao, H. Nakai, T. Vreven, K. Throssell, J. A. Montgomery, Jr., J. E. Peralta, F. Ogliaro, M. J. Bearpark, J. J. Heyd, E. N. Brothers, K. N. Kudin, V. N. Staroverov, T. A. Keith, R. Kobayashi, J. Normand, K. Raghavachari, A. P. Rendell, J. C. Burant, S. S. Iyengar, J. Tomasi, M. Cossi, J. M. Millam, M. Klene, C. Adamo, R. Cammi, J. W. Ochterski, R. L. Martin, K. Morokuma, O. Farkas, J. B. Foresman and D. J. Fox, *Gaussian~16 Revision C.01*, Gaussian Inc., Wallingford CT, 2016.
43 F. Neese, *Wiley Interdiscip. Rev.: Comput. Mol. Sci.*, 2012, **2**, 73–78.
44 J. Wagner, P. Zimmermann Crocomo, M. A. Kochman, A. Kubas, P. Data and M. Lindner, *Angew. Chem., Int. Ed.*, 2022, **134**, e202202232.
45 G. Ricci, A. Landi, J. C. Sancho-Garca and Y. Olivier, *Adv. Opt. Mater.*, 2024, 2402765, DOI: **10.1002/adom.202402765**.
46 L. De Thieulloy, L. E. De Sousa and P. De Silva, Enhancing Triplet Harvesting in Inverted Singlet–Triplet Gap Molecules through Mechanistic Understanding, 2025, **https://chemrxiv.org/engage/chemrxiv/article-details/67c011156dde43c908ad7530**.
47 J. Terence Blaskovits, M. H. Garner and C. Corminboeuf, *Angew. Chem., Int. Ed.*, 2023, **62**, e202218156.
48 A. Majumdar, S. Das and R. Ramakrishnan, Unlocking Inverted Singlet–Triplet Gap in Alternant Hydrocarbons with Heteroatoms, 2025, **https://arxiv.org/abs/2503.20369**.
49 S. J. Stoneburner, J. Shen, A. O. Ajala, P. Piecuch, D. G. Truhlar and L. Gagliardi, *J. Chem. Phys.*, 2017, **147**, 164120.
50 P. Ertl and A. Schuffenhauer, *J. Cheminf.*, 2009, **1**, 1–11.
51 D. Farquhar and D. Leaver, *J. Chem. Soc. D*, 1969, 24–25.
52 M. Melle-Franco, *Chem. Commun.*, 2015, **51**, 5387–5390.
53 T. Sutradhar and A. Misra, *J. Phys. Chem. A*, 2018, **122**, 4111–4120.
54 J. Souza, L. Benatto, G. Candiotto, L. Roman and M. Koehler, *J. Phys. Chem. A*, 2022, **126**, 1393–1402.
55 T. Shen, D. Chen, L. Lin and J. Zhu, *J. Am. Chem. Soc.*, 2019, **141**, 5720–5727.
56 A. DeFusco, N. Minezawa, L. V. Slipchenko, F. Zahariev and M. S. Gordon, *J. Phys. Chem. Lett.*, 2011, **2**, 2184–2192.
57 W. Tao, Z. Zhao, J. Kang, Z. Li, J. Zhu, Y. Zuo, M. Huang, J. Cui, J. Yu and Y. Liu, *et al.*, *J. Photochem. Photobiol., A*, 2025, **459**, 115992.

58 J. Fan, L. Lin and C.-K. Wang, *Phys. Chem. Chem. Phys.*, 2017, **19**, 30147–30156.
59 R. Pollice, P. Friederich, C. Lavigne, G. dos Passos Gomes and A. Aspuru-Guzik, *Matter*, 2021, **4**, 1654–1682.
60 G. Ricci, E. San-Fabián, Y. Olivier and J. C. Sancho-García, *ChemPhysChem*, 2021, **22**, 553–560.
61 L. Wrigley and C. W. Schlenker, *Annu. Rev. Phys. Chem.*, 2025, **76**, 329–355.